JCTC Journal of Chemical Theory and Computation

pubs.acs.org/JCTC Article

Analogy between Boltzmann Machines and Feynman Path Integrals

Srinivasan S. Iyengar* and Sabre Kais*

Cite This: J. Chem. Theory Comput. 2023, 19, 2446−2454

Read Online

ACCESS | Metrics & More | Article Recommendations

ABSTRACT: Machine learning has had a significant impact on multiple areas of science, technology, health, and computer and information sciences. Through the advent of quantum computing, quantum machine learning has developed as a new and important avenue for the study of complex learning problems. Yet there is substantial debate and uncertainty in regard to the foundations of machine learning. Here, we provide a detailed exposition of the mathematical connections between a general machine learning approach called Boltzmann machines and Feynman's description of quantum and statistical mechanics. In Feynman's description, quantum phenomena arise from an elegant, weighted sum over (or superposition of) paths. Our analysis shows that Boltzmann machines and neural networks have a similar mathematical structure. This allows the interpretation that the hidden layers in Boltzmann machines and neural networks are discrete versions of path elements and allows a path integral interpretation of machine learning similar to that in quantum and statistical mechanics. Since Feynman paths are a natural and elegant depiction of interference phenomena and the superposition principle germane to quantum mechanics, this analysis allows us to interpret the goal in machine learning as finding an appropriate combination of paths, and accumulated path-weights, through a network, that cumulatively captures the correct properties of an x-to-y map for a given mathematical problem. We are forced to conclude that neural networks are naturally related to Feynman path-integrals and hence may present one avenue to be considered as quantum problems. Consequently, we provide general quantum circuit models applicable to both Boltzmann machines and Feynman path integrals.

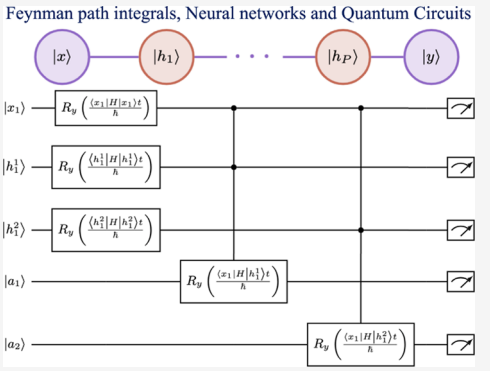

1. INTRODUCTION

Machine learning[1] has had significant impact on multiple areas of science, technology, health, and computer and information sciences. These approaches have recently become popular in modeling molecular systems, with a particular increase in interest following Google DeepMind's seemingly triumphant[2,3] efforts toward protein structure prediction. Through the advent of quantum computing, quantum machine learning has developed as an important avenue for the study of complex learning problems. A neural-network ansatz trainable method on a quantum and/or classical device has been used with unprecedented success in procuring a reasonable approximation of a target quantum state.[4] Of particular interest and with a great success is the use of the Restricted-Boltzmann Machine (RBM).[5] The choice of RBM is due to the fact it has been proven to be a universal approximator for any probability density[5−7] and has received astonishing success in simulating a wide variety of drivers in condensed-matter physics,[8,9] quantum dynamics[10] vibration spectroscopy of molecular systems,[11,12] quantum chemistry[13−18] of complex multiscale problems,[19] and even in standard classification tasks.[20,21] Prior work has also established that RBM is capable of mimicking a volume-law entangled quantum state even when sparsely parametrized.[22] With quadratically scaling quantum circuits available,[13] RBM also shows hints of possible quantum advantage due to proven intractability of polynomially retrieving the full distribution classically.[23] Graph-based[18] projection operators that resolve the identity[17,24] have been used to construct RBMs for correlated electronic potential energy surfaces[16] and reduce the computational complexity for classical[17,25] and quantum[24] calculations.

Even though RBMs (and neural networks in general) have been widely used, probing into the underlying learning mechanism and the connection to a Feynman path integral RBM is still sparsely explored.[26] In this paper, we explore a deep mathematical and conceptual connection between RBM, Feynman path integrals, and more generally neural networks. This step is especially critical considering that, arguably, the most general, conceptually elegant, and unifying formalism of both quantum mechanics and statistical mechanics appears through Feynman's description of path integrals.[27,28] For a

Received: February 23, 2023
Published: April 26, 2023

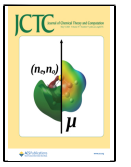

https://doi.org/10.1021/acs.jctc.3c00187
J. Chem. Theory Comput. 2023, 19, 2446−2454

historical view of path integrals, see ref 29, and for applications to other areas, see ref 30. Over the years, Feynman path integrals have been the workhorse for many path integral-based molecular dynamics[31,32] and Monte Carlo[33,34] formalisms to compute equilibrium properties in condensed phase quantum systems.[35,36] The real time interpretation of Feynman path integrals have been the basis for powerful numerical procedures such as centroid molecular dynamics[37−39] and ring-polymer molecular dynamics.[40]

The paper is organized as follows: In Section 2 we present a brief summary of RBMs which is followed by developing explicit connections between Feynman path integrals, RBMs, and neural networks in general in Sections 3 and 4. As a direct consequence of the analysis in Section 4, we are able to provide general quantum circuit models that are applicable to both Boltzmann machines and to Feynman path integral descriptions. Based on this description, in Section 6, we are able to provide a discussion on *k*-local Hamiltonians which yield full Boltzmann machine (unrestricted) and finally in Section 4.1, we present one interpretation of this mathematical exposition based on inverse scattering theory. Conclusions are given in Section 9.

2. RESTRICTED-BOLTZMANN MACHINE

The network of the Restricted-Boltzmann Machine denoted as G involves two interconnected spin registers $G = (V_1, V_2, E)$, where the vertex set $V_1=\{v\}_{i=1}^{i=n}$ with n $\in\mathbb{Z}_+$, and each is associated with an operator $\sigma_z(v_i)$. A similar prescription exists for $V_2=\{h\}_{i=1}^{i=p}$ with p $\in\mathbb{Z}_+$, and each is associated with an operator $\sigma_z(h_i)$. The network is described in Figure 1. The set of

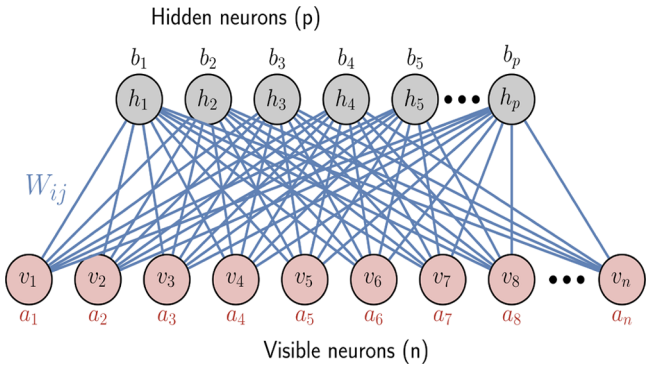

Figure 1. RBM network G = (V,E) showing the biases $\vec{a}$ and $\vec{b}$ for hidden $\{h_j\}_{j=1}^{p}$ (gray) and visible $\{v_i\}_{i=1}^{n}$ (red) neurons and the interconnecting weights W_{ij} (blue).

edges $|E| = p*n$ and is weighted by W_j^i. The Hamiltonian of the network is

$$\mathcal{H}(\vec{X}, \vec{v}, \vec{h}) = \sum_{i=1}^{n} a_i\sigma^z(v_i) + \sum_{j=1}^{p} b_j\sigma^z(h_j) + \sum_{i=1,j=1}^{n,p} W_j^i\sigma^z(v_i)\sigma^z(h_j) \tag{1}$$

and the corresponding thermal state the network encodes is

$$\rho_G^C(\vec{X}, \vec{v}, \vec{h}) = \frac{e^{-\mathcal{H}(\vec{X},\vec{v},\vec{h})}}{Tr_{\{v,h\}}e^{-\mathcal{H}(\vec{X},\vec{v},\vec{h})}} \tag{2}$$

where the superscript C denotes the classically correlated thermal state. Using eq 2, one can define a proxy state/ansatz for the target quantum state as

$$\psi(\vec{X})_H = \sqrt{\sum_{\vec{h}} \mathrm{diag}(\rho_G^C(\vec{X}, \vec{v}, \vec{h}))} \tag{3}$$

of the driver Hamiltonian $H \in C^{d\times d}$ where $\vec{X}$ can be variationally trained. Using the RBM network, we have shown that one can obtain very accurate electronic structures of simple molecules and band structures of two-dimensional materials.[13,14]

3. CONNECTIONS BETWEEN RESTRICTED BOLTZMAN MACHINES AND FEYNMAN PATH INTEGRALS

The starting point in our discussion of Feynman path integrals for quantum and statistical mechanics is the quantum propagator in real and imaginary time given by

$$\rho_{x,x'} \equiv \langle x|\exp\{-\beta H\}|x'\rangle \tag{4}$$

where, when β is real, $\rho_{x,x'}$ represents the quantum canonical density operator, and β becomes the inverse temperature or $\beta = 1/k_BT$. When β is imaginary, that is, $\beta = it/\hbar$, $\rho_{x,x'}$ represents the real time evolution or unitary propagation of the problem. This process of connecting real time and imaginary inverse temperature values is commonly known as Wick rotation[28] on the complex time frame and is one hallmark of quantum statistical mechanics within Feynman's description. At this stage, it is also critical to note that $|x\rangle$ may represent any basis, continuous or discrete, and we make no distinction of this in our discussion.

The next step in Feynman's exposition of path integrals is to slice the propagator in eq 4 into small increments[34] given by $\delta\beta = \beta/P$. Thus, for Hamiltonians that only contain two-body terms,

$$\begin{aligned}\rho_{x,x'} &\equiv \langle x|[\exp\{-\delta\beta H\}]^P|x'\rangle \\ &= \langle x|[\exp\{-\delta\beta H\}][\exp\{-\delta\beta H\}]\cdots P \text{ terms}|x'\rangle\end{aligned} \tag{5}$$

a family of resolutions of identity $\int dh_i|h_i\rangle\langle h_i|$ inserted between the P propagation slices yields

$$\begin{aligned}\rho_{x,x'} = \int dh_1dh_2\cdots &\langle x|[\exp\{-\beta H\}]|h_1\rangle \\ &\langle h_1|[\exp\{-\beta H\}]|h_2\rangle\langle h_2|\cdots|h_P\rangle \\ &\langle h_P|[\exp\{-\beta H\}]|x'\rangle\end{aligned} \tag{6}$$

which has the beautiful interpretation according to Feynman[28] of the particle "traveling" from x to x' in a series of steps h_1, h_2, ..., h_P, which define a path, with the total amplitude on the left side being a sum over all such paths. In the discrete representation, eq 6 may be written as

$$\begin{aligned}\rho_{x_\alpha,x_{\alpha'}} = \sum_{\bar{\mu}} &\langle x_\alpha|[\exp\{-\beta H\}]|h_1^{\mu_1}\rangle \\ &\prod_{i=1}^{P}\langle h_i^{\mu_i}|[\exp\{-\beta H\}]|h_{i+1}^{\mu_{i+1}}\rangle \\ &\langle h_P^{\mu_P}|[\exp\{-\beta H\}]|x_{\alpha'}\rangle\end{aligned} \tag{7}$$

where $\bar{\mu} \equiv \{\mu_1, \mu_2, ..., \mu_P\}$, and μ_i represents the μ_ith discretization of the ith slice in the Feynman path integral. That is, each of the P slices are discretized as noted, and these

https://doi.org/10.1021/acs.jctc.3c00187
J. Chem. Theory Comput. 2023, 19, 2446−2454

discreizations are labeled using $\{\mu_i\}$. Thus, in essence, eq 7 is simply a discrete sum over paths labeled by $\bar{\mu}$, or more specifically, the sequence of indices $\{x_\alpha, h_1^{\mu_1}, h_2^{\mu_2}, \cdots h_P^{\mu_P}, x_{\alpha'}\}$ represents one specific path that connects x to x'. As the number of slices $P \to \infty$, this then leads to the sum over paths notation of Feynman given by

$$\rho_{x,x'} = \int \mathcal{D}h \langle x|[\exp\{-\beta H\}]|x'\rangle \tag{8}$$

and the expression above is essentially a sum over paths, or path integral over the path variable h, as in eq 7, and the path integral description is over basis vectors $\{|h_i\rangle\}$ beginning from $|x\rangle$ and ending at $|x'\rangle$.. The paths are traversed by the evolution process described by the operator $\exp\{-\beta H\}$. Thus, the interference of, or sum over, paths, leading to the superposition theorem which is a hallmark of quantum theory, appears in Feynman's description through the accumulation of all possible paths described in eqs 7 and 8. Additionally when the outer indices $|x\rangle$ and $|x'\rangle$ are on different spaces, the expression above presents a more general path integration form for $|x\rangle \to |y\rangle$. Equations 7 and 8 may be compactly represented using Figure 2. The case where $|x\rangle \to |y\rangle$. is shown in Figure 3 and in a more verbose manner in Figure 4 where the discrete version in eq 7 is spelt out. In all cases, $|x\rangle$ and $|h_i\rangle$ represent vector spaces, and hence, the similarity between Figures 2, 3, and 4, and restricted Boltzmann machines (Figure 1) from machine learning, is palpable. These connections are further explored in the following sections.

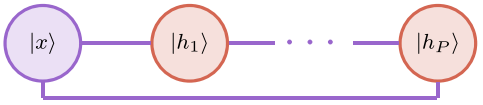

Figure 2. Neural network depiction of eq 8.

Figure 3. Neural network depiction of eq 8. Similar to Figure 2, but now $|x'\rangle$ is assumed to be a different space from $|x\rangle$. This figure is elaborated in Figure 4 to make connections to the sum of path, eq 7.

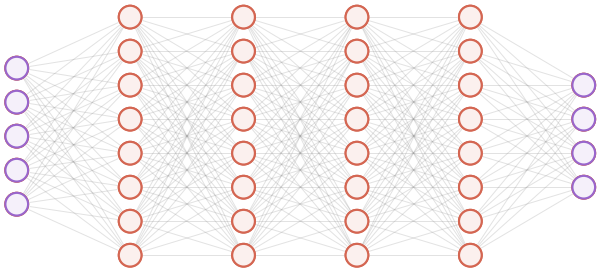

Figure 4. Explicit version of Figure 3 that connects directly to sum over paths description on eq 7.

Furthermore, in Feynman's description, when β is chosen to be real, that is inverse temperature $(= 1/k_B T)$, the quantity,

$$\mathcal{Z} = \mathrm{Tr}[\rho] = \int dx \mathcal{D}h \langle x|[\exp\{-\beta H\}]|x\rangle \tag{9}$$

is the partition function, and the quantity $\rho_{x,x'}/Z$ is canonical weight which depends on all the layers as per eq 6 and all possible paths as per eq 7.

4. RESTRICTED BOLTZMANN MACHINES RECAST USING FEYNMAN'S PATH INTEGRALS

To connect the formalism above to Boltzmann machines and neural networks in general, we may begin by interpreting the family of basis states $\{|x\rangle\}$ as *visible* layer states, and the layers $\{|h_i\rangle\}$ as *hidden* layer states. For more general neural networks $|x'\rangle$ may be replaced by $|y\rangle$. When this is not the case, there are multiple hidden layers and one visible layer, as denoted in Figures 1 and 2. One must note that in the traditional description of Feynman path integrals, there is no distinction between the variables used to describe the states $\{|x\rangle\}$ and $\{|h_i\rangle\}$ as these are both treated as belonging to the same Hilbert space. Here, we choose to highlight the difference between path states, $\{h_i\}$, and terminal states, $\{|x\rangle\}$, to make the connections to Boltzmann machines explicit. In such a situation, the formalism in eqs 6, 7, and 8 yields the realization of a sum over all paths that begin at the visible basis state $|x\rangle$ and terminate at the visible basis state $|x'\rangle$ by traversing through all the *hidden* basis points (eq 7) depicted as $\{|h_i\rangle\}$. Furthermore, the evolution along these paths is dictated by $\exp\{-\beta H\}$, and specifically by the Hamiltonian H.

To parametrize such an evolution process we may introduce the needed Hamiltonian that depicts the dynamics in eq 8 as

$$\begin{aligned} H = & \int dx dx' |x\rangle\langle x|H|x'\rangle\langle x'| + \\ & \sum_{i=1}^{P} \int dh_i |h_i\rangle\langle h_i|H|h_i\rangle\langle h_i| + \\ & \int dx dh_1 |x\rangle\langle x|H|h_1\rangle\langle h_1| + \\ & \sum_{i>1}^{P} \int dh_i dh_{i+1} |h_i\rangle\langle h_i|H|h_{i+1}\rangle\langle h_{i+1}| + \\ & \int dx dh_P |h_P\rangle\langle h_P|H|x\rangle\langle x| + c.c. \end{aligned} \tag{10}$$

and in this general form, the connections are apparent to eq 1. We note that this also represents a *continuous* neural network with P hidden layers (compare Figures 1 and 2), where the diagonal elements of H are biases applied to each (visible and hidden) state, and the off-diagonal elements in H are coupling elements across basis states, referred to as weights, either within a given visible layer, or across neighboring layers. The discrete form of this Hamiltonian may be simply obtained by using a finite number of basis functions for visible and hidden layers (eq 7), and the integrals then become summations leading to matrix elements

$$\begin{aligned} \text{Biases:} \quad & \{\langle x_\alpha|H|x_\alpha\rangle;\ \langle h_i^{\mu_i}|H|h_i^{\mu_i}\rangle\} \\ \text{Weights:} \quad & \{\langle x_\alpha|H|h_1^{\mu_1}\rangle;\ \langle h_i^{\mu_i}|H|h_{i+1}^{\mu_{i+1}}\rangle\} \end{aligned} \tag{11}$$

and

https://doi.org/10.1021/acs.jctc.3c00187
J. Chem. Theory Comput. 2023, 19, 2446−2454

$$H = \sum_{\alpha} \langle x_\alpha|H|x_\alpha\rangle\{|x_\alpha\rangle\langle x_\alpha|\} + \sum_{i,\mu_i} \langle h_i^{\mu_i}|H|h_i^{\mu_i}\rangle\{|h_i^{\mu_i}\rangle\langle h_i^{\mu_i}|\} + \sum_{\alpha,\mu_1} \langle x_\alpha|H|h_1^{\mu_1}\rangle\{|x_\alpha\rangle\langle h_1^{\mu_1}|\} + c.c. + \sum_{i>1}^{P} \sum_{i,\mu_i,\mu_{i+1}} \langle h_i^{\mu_i}|H|h_{i+1}^{\mu_{i+1}}\rangle\{|h_i^{\mu_i}\rangle\langle h_{i+1}^{\mu_{i+1}}|\} + c.c. + \sum_{\alpha',\mu P} \langle x_{\alpha'}|H|h_P^{\mu_P}\rangle\{|x_{\alpha'}\rangle\langle h_P^{\mu_P}|\} + c.c. \quad (12)$$

which is a generalization of eq 1, derived from eq 10. In eq 12, the terms, $\{|x_\alpha\rangle\langle x_\alpha|\}$; $\{|h_i^{\mu_i}\rangle\langle h_i^{\mu_i}|\}$; ⋯, are projectors that are replaced by the Pauli operators in eq 1. In such a situation, eq 8 represents the evolution process of quantum mechanics but also the learning process of machine learning. The weights for such a learning process arise from the Hamiltonian, eqs 10, 11, and 12. Equation 10 is clearly a generalization to eq 1 for an arbitrary number of layers and essentially a continuous set of vertices in each layer, with eq 12 representing the discretized version.

Additionally, we note the close connection[41] between eqs 1 and 12 and the quantum Ising Model that has been studied widely on diverse quantum hardware platforms such as trapped ions,[42] Rydberg atoms,[43] polar molecules,[44] cold atomic gases,[45] and superconducting circuits.[46] In its full implementation, the quantum Ising Model Hamiltonian with local magnetic fields may be written as

$$H_{IT} = \sum_{\gamma} \sum_{i<j} J_{ij}^{\gamma} \sigma_i^{\gamma} \sigma_j^{\gamma} + \sum_{\gamma} \sum_{i} B_i^{\gamma} \sigma_i^{\gamma} \quad (13)$$

where $\gamma \in (x, y, z)$, J_{ij}^{γ} is the coupling between sites i and j along the γ direction, B_i^{γ} is the local magnetic field at site i along the γ direction, and the quantities $\{\sigma_i^{\gamma}\}$ are the Pauli spin operators acting on the ith lattice site along the γ-direction of the Bloch sphere. The critical distinction between eqs 1 and 13 is that, in principle, all sites are connected to each other in eq 13, and hence, H_{IT} is closer to a full Boltzmann machine.

The cost function of RBMs (see eq 2) arise in eq 7 when β is real. Such a situation may also be realized upon inspection of Figure 3, where each node is to be interpreted as a single layer of nodes, and the wires connecting nodes depict *all* weights across layers, or a linear map between the same (see Figure 4). These figures now summarize the analogy between Feynman's description of quantum and statistical mechanics and machine learning models as presented using Boltzmann machines.

In the current form, the Hamiltonian in eq 10 also appears to have similarities to Ising model Hamiltonians. Compare eqs 10, 11, 12, 13, and 1. But what is missing here is what is known as activation functions common in machine learning, which we may simply be interpreted as connections of the hidden bases to bath vectors, or dissipative variables. This aspect is treated in further detail in Section 7.

4.1. Boltzmann Machines as an Inverse Scattering Problem: "Interpretability" of the "Hidden" Layer. In the above sections, we discussed the theory of Feynman path integrals as applicable to both quantum mechanics as well as statistical mechanics. This naturally leads to the introduction of a set of intermediate states, depicted as $\{|h_i\rangle\}$ above, that are visited during transitions both in real time (quantum mechanics) and imaginary time (statistical mechanics and thermodynamics). We then showed how the exact same structure appears in Boltzman machines and in neural networks thus leading to one obvious interpretation that perhaps Boltzman machines are a realization of Feynman path integrals. This will automatically leads to definitions for entropy through partial trace over hidden layers, in Section 5, and similar definitions for higher order interactions, Section 6.

However, we now ask if we may expound upon an equivalent description for the definition of weights and biases, as alluded to in eq 11, as these appear in machine learning. In machine learning and Boltzmann machines, a network such as that in Figure 4 is represented by

$$|h_{a+1}\rangle = f_{a+1}(\mathcal{W}_{a,a+1}|h_a\rangle) \quad (14)$$

where f_{a+1} represents the activation function for the $(a + 1)$-th layer, and $\{\mathcal{W}_{a,a+1}\}$ are the weight tensors (including bias) connecting the a-th and $(a + 1)$-th layers. In defining $\{\mathcal{W}_{a,a+1}\}$ here, we have combined the $\{b_j; W_j^i\}$ terms in eq 1. The functions, f_{a+1}, are chosen to be functions of the kets created by the action $[\mathcal{W}_{a,a+1}|h_a\rangle]$, and thus, the weights $\{\mathcal{W}_{a,a+1}\}$ are operators that act on kets. The assumption here is that f_i are analytic, differentiable functions, and hence, continuous representations of ReLU are acceptable forms. For the description in Section 3,

$$\langle h_{a+1}|[\exp\{-\delta\beta H\}]|h_a\rangle \equiv \langle h_{a+1}|f_{a+1}(\mathcal{W}_{a,a+1}|h_a\rangle) \quad (15)$$

and this is the key central insight that appears from the treatment in Section 3 and crystallizes the analogy presented in this paper. Thus, influenced by eq 6, an equivalent description for the machine learning processes described by Figures 3 and 4 may be written in the continuous limit as

$$|y\rangle = \int dh_1 dh_2 \cdots f_{P+1}(\mathcal{W}_{P+1,P}|h_P\rangle) \langle h_P|f_P(\mathcal{W}_{P,P-1}|h_{P-1}\rangle)\langle h_{P-1}|\cdots|h_2\rangle \langle h_2|f_2(\mathcal{W}_{1,2}|x\rangle) \quad (16)$$

Note the close similarity between eqs 6 and 16 where both seem to now have a sum over paths flavor. Clearly, whereas in quantum dynamics eq 6 may be computed by providing a system Hamiltonian, in machine learning, the weights, $\{\mathcal{W}_{a,a+1}\}$, are to be obtained based on a known set of transitions, $|y\rangle \leftarrow |x\rangle$ that are used for training the network. Thus, in a sense, the ML approach to Boltzman machines is one where the Hamiltonian is computed based on a data set that captures the $|y\rangle \leftarrow |x\rangle$ map.

Hence, to achieve an equivalent description for the weights, $\{\mathcal{W}_{a,a+1}\}$, we may remind ourselves that in quantum dynamics and scattering theory,[47] the transition amplitude, $\langle\chi_f|\Omega|\chi_i\rangle$ under the influence of the Möller operator, Ω, which includes time evolution (as in Section 3) or associated Greens function,[47] is the key aspect and connects to various observables such as state-to-state scattering probabilities, rate constants, and also vibrational properties. By comparison this statement is not dissimilar to that in eqs 6 and 16, but in fact from this perspective, the machine learning problem is an inverse scattering problem in that, one may say, the Hamiltonian for the process, given by eqs 10, 11, and 12, needs to be discovered. In this language, the "hidden" layers of machine learning are

https://doi.org/10.1021/acs.jctc.3c00187
J. Chem. Theory Comput. 2023, 19, 2446−2454

simply the steps needed to construct the interference experiments germane to quantum mechanics. Whereas in quantum mechanics these "hidden" steps seem to allow the system to achieve a probabilistic view, in machine learning the same probabilistic view samples a large parameter space thus allowing for an optimal solution to a given (hard) problem.

5. DESCRIPTION OF ENTROPY

To describe the entropy of the system containing $\{|x\rangle; \{|h_i\rangle\}\}$, using eq 9, we may first define the marginal probabilities using the matrix elements

$$\rho_{x,h_1} = \langle x|[\exp\{-\delta\beta H\}]|h_1\rangle \tag{17}$$

and

$$\rho_{h_i,h_{i\pm1}} = \langle h_i|[\exp\{-\delta\beta H\}]|h_{i\pm1}\rangle \tag{18}$$

to redefine eq 7 and eq 8 as

$$\rho_{x,x'} = \int dh_1 dh_2 \cdots \rho_{x,h_1}\rho_{h_1,h_2}\cdots \tag{19}$$

These marginals may be used to write the Shannon entropy functions: $\mathcal{S}[\rho_{x,h_1}]$, and $\mathcal{S}[\rho_{h_i,h_{i\pm1}}]$. The overall entropy of the network is obtained using the entropy of each layer in a manner similar to the inclusion exclusion principle in set theory,[48] an appropriate generalization for which is provided by Bethe's free energy[49] and may be written as

$$\mathcal{S}[\rho_x] + \sum_i \mathcal{S}[\rho_{h_i}] - \mathcal{S}[\rho_{x,h_1}] - \sum_i \mathcal{S}[\rho_{h_i,h_{i+1}}] \tag{20}$$

which is often referred to as mutual information entropy and also has applications in Belief propagation.[49] For the special case of the network in Figure 1, eq 20 reduces to

$$\mathcal{S}[\rho_x] + \mathcal{S}[\rho_{h_1}] - \mathcal{S}[\rho_{x,h_1}] \tag{21}$$

which is consistent with the expression in ref 50. However, eq 20 provides a generalization for an arbitrary number of hidden layers for more general RBMs beyond those in Figure 1.

6. *K*-LOCAL HAMILTONIANS YIELD BOLTZMANN MACHINES

For cases where the Hamiltonian in eq 10 has k-body terms, the situation in eqs 8, 19, and 20 is more complicated. For example, for three-body terms in eq 10, the expression in eq 19 may be written as

$$\rho_{x,x'} = \int dh_1 dh_2 \cdots \rho_{x,h_1,h_2}\rho_{h_1,h_2,h_3}\cdots\rho_{h_{p-1},h_p,x'} \tag{22}$$

The associated neural network and Feynman path integration techniques are both represented in compact form in Figure 5. Here, each triangle captures a three-body interaction, and this aspect is referred to using the blue squares inside the triangles. For example, the three-body terms make the Hamiltonian tensorial, and thus, it simultaneously interacts bases $\{\vec{x}; \overrightarrow{h_1}; \overrightarrow{h_2}\}$, etc. While a tree-type topology may be appropriate in such cases as the interactions grow, a simplified form of the representation is presented in Figure 5. Again, as in Figure 3, when the outer indices $|x\rangle$ and $|x'\rangle$ are on different Hilbert spaces, $|x'\rangle$ in eq 22 is replaced with $|y\rangle$. The associated depiction is provided in Figure 6. It must be noted that Figure 5 is not a restricted Boltzmann machine as may be seen from the fact that

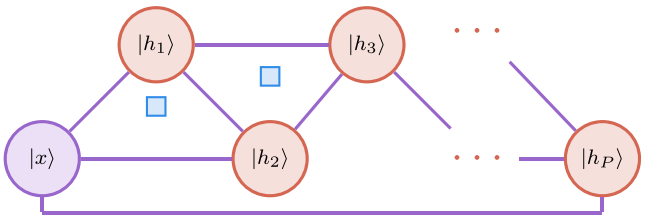

Figure 5. 3-Local neural network depiction with entropy in eq 23. Each triangle represents a rank-3 weight tensor and is depicted with a blue square on its interior. In general, this could be a partial tree topology but is presented here in a simplified form.

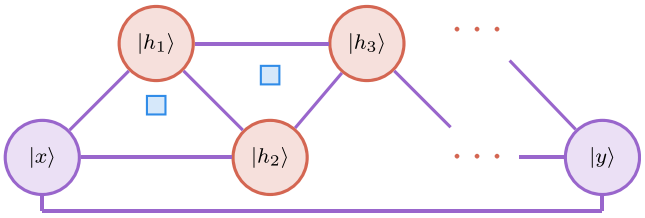

Figure 6. Same as Figure 5 but now depicts the case for $|x\rangle \to |y\rangle$ as in Figure 3.

the layer corresponding to $|x\rangle$ is connected to two following layers corresponding to $|h_1\rangle$ and $|h_2\rangle$, and so on. In fact, this is a step toward a general Boltzmann machine, and as the many-body interactions captured within the Hamiltonian increases, this approaches the path integral formalism commensurate with the full Boltzmann machine.

In such cases a generalization to the entropy from eq 20 may be obtained from Kekuchi's theory.[49] We begin this generalization by reinspecting Figures 5 and 6. These figures contain sets of triangles that are connected to each other since the Hamiltonian contains three-body terms. Thus, higher order Hamiltonians will necessitate the presence of higher order simplexes[51] that are connected, and these will be commensurate with the many-body interaction terms that are captured within the Hamiltonian. Thus, it is appropriate to think of the Boltzmann machine in Figures 5 and 6 as graphs such that when the Hamiltonian contains k-body terms, the associated Boltzmann machine would have k-nodes that are completely connected and hence best represented as k-simplexes. Thus, if we consider the resultant neural network as a graph made of simplexes, or as a simplicial complex,[51,52] the entropy arises from a graph theoretic description[18,49,53] and may be written as

$$\sum_{\alpha,r}^{\mathcal{R}} (-1)^r \mathcal{S}_{\alpha,r}\mathcal{M}_{\alpha,r} \tag{23}$$

Here, the αth rank-r simplex within the graph created from the neural network has entropy $\mathcal{S}_{\alpha,r}$, which may be thought to be a functional of the reduced probability $\rho_{\alpha,r}$, that is the reduced probability for the αth rank-r simplex in a graphical depiction such as that in Figures 5 and 6. The quantity $\mathcal{R}$ in eq 23 is the maximum rank of the simplexes that is the $\mathcal{R} = k$ for k-local Hamiltonians. Thus, for the two-body case, the rank of the objects within a graphical description of the neural network is "r = 0" (nodes in the network) and "r = 1" (edges in the network). For the three-body case in Figures 5 and 6, the value of $\mathcal{R}$ is 2, and the corresponding entropy takes the form

https://doi.org/10.1021/acs.jctc.3c00187
J. Chem. Theory Comput. 2023, 19, 2446−2454

$$\sum_{\alpha\in\text{nodes}} \mathcal{S}_{\alpha,0}\mathcal{M}_{\alpha,0} - \sum_{\alpha\in\text{edges}} \mathcal{S}_{\alpha,1}\mathcal{M}_{\alpha,1} + \sum_{\alpha\in\text{faces}} \mathcal{S}_{\alpha,2}\mathcal{M}_{\alpha,2} \tag{24}$$

where the set of "nodes" include visible and hidden layers, the set of "edges" include connections between the same and are determined by the traditional weights used in machine learning, and finally, the set of "faces" include generalized weights that now depend on three sets of layers that may be any combination of visible or hidden layers.

The quantity, $\mathcal{M}_{\alpha,r}$ in eq 23 is a multiplicity term and prevents overcounting in the graph-theoretic expression, eq 23, and includes the number of times the αth (r)-rank object appears in all simplexes of rank greater than or equal to r. Thus, through the analogy discussed we are also able to provide high-order neural networks as a extension of Feynman path integrals with Hamiltonians that may contain higher order terms.

7. ROLE OF ACTIVATION FUNCTIONS

In Boltzmann machines and neural networks, there is a concept called activation functions, which has thus far been ignored in our discussion. One can interpret such activation functions as a external bath, that perform the operation that modifies eq 6 by replacing

$$|h_P\rangle\langle h_P|[\exp\{-\delta\beta H\}]|x'\rangle \rightarrow f_{act}(|h_P\rangle\langle h_P|[\exp\{-\delta\beta H\}]|x'\rangle) \tag{25}$$

and

$$|h_2\rangle\langle h_2|\cdots|x'\rangle \rightarrow f_{act}(|h_2\rangle\langle h_2|\cdots|x'\rangle) \tag{26}$$

and so on. Here, for each hidden node, the activation function attenuates the probability at that node, through connection to an external bath, as shown in Figure 7 thus modifying the Hamiltonian in eq 10 to read

$$H_{activation} = H + \left(\sum_{i=1}^{P}\int dh_i ds_i |h_i\rangle\langle h_i|H|s_i\rangle\langle s_i| + c.c.\right) + \left(\sum_{i=1}^{P}\int ds_i |s_i\rangle\langle s_i|H|s_i\rangle\langle s_i| + c.c.\right) \tag{27}$$

Thus, we map the situation with actvation functions to include bath variables as is expected for system-bath or condensed phase quantum dynamics[54]

However, it is also to be noted that the most general form of the Hamiltonian achievable within ion trap quantum hardware

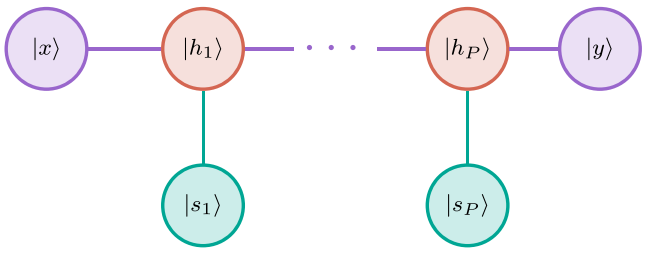

Figure 7. Neural network with activation function depicted using bath variables. See Section VII. One my view this as a special case of the k-local description provided in Section VI and Figure 6.

represents a case very similar to eq 27. In the language of spin and boson operators,[55]

$$\mathcal{H}^{Ion-Trap} = \mathcal{H}^{IT}_{system} + \mathcal{H}^{IT}_{interaction} + \mathcal{H}^{IT}_{bath} \tag{28}$$

where the three individual terms may be considered as mappable to the three parts of eq 27 ,and while $\mathcal{H}^{IT}_{system}$ has an identical definition as in eq 13, bath components have the form

$$\mathcal{H}^{IT}_{bath} = \sum_{\alpha} N_\alpha a^\dagger_\alpha a_\alpha$$
$$\mathcal{H}^{IT}_{interaction} = \sum_{\gamma,\alpha,i} \kappa_\alpha \sigma^\gamma_i (a_\alpha + a^\dagger_\alpha) \tag{29}$$

Here, as usual, σ^γ_i are the Pauli spin operators for the ith spin acting along the γ direction of the Bloch sphere, and a_α and $a^\dagger_\alpha$ are phonon annihilation and creation operators for vibrational mode α. In eqs 28, κ_α describes the coupling strength between the effective spin-1/2 system and a quantum harmonic bath, which contains N_α phonons in mode α.

Thus, while the paper is primarily based on exposing the analogy between Boltzmann machines and Feynman path integrals, it is also evident through the connections between eqs 10 and 13 on the one hand, and eqs 27 and 28 on the other hand, that quantum computing implementations may be developed in future that may have similar algebraic structure for machine learning problems as well as quantum chemical dynamics problems.

8. QUANTUM CIRCUIT DESCRIPTIONS FOR BOLTZMANN MACHINES AND PATH INTEGRALS

In Figure 8, we present a circuit model for both the RBM shown and also for the Feynman path integral that is represented by Figure 8(a). In this quantum circuit, the single-qubit R_y gates acting only on the visible and hidden units have rotation angles parametrized by the matrix elements as shown in the figure, the biases in eq 11, and are responsible for creating the noninteracting part of the distribution, that is

$$\bigotimes_\alpha \left[\exp\left\{\frac{-\imath\langle x_\alpha|H|x_\alpha\rangle t}{\hbar}\right\}|x_\alpha\rangle\right]\bigotimes_{i,\mu_i}\left[\exp\left\{\frac{-\imath\langle h_i^{\mu_i}|H|h_i^{\mu_i}\rangle t}{\hbar}\right\}|h_i^{\mu_i}\rangle\right] \equiv \bigotimes_\alpha \left[R_y\left(\frac{\langle x_\alpha|H|x_\alpha\rangle t}{\hbar}\right)|x_\alpha\rangle\right]\bigotimes_{i,\mu_i}\left[R_y\left(\frac{\langle h_i^{\mu_i}|H|h_i^{\mu_i}\rangle t}{\hbar}\right)|h_i^{\mu_i}\rangle\right] \tag{30}$$

while the interaction terms are turned on through using CCR_y gates acting on an ancilla register as the target. For example, after the first CCR_y gates, the resultant state is

$$\begin{aligned}
&|a_1\rangle\bigotimes_\alpha|0_\alpha\rangle\langle 0_\alpha|R_y\left(\frac{\langle x_\alpha|H|x_\alpha\rangle t}{\hbar}\right)|x_\alpha\rangle\bigotimes_{i,\mu_i}|0_{i,\mu_i}\rangle\langle 0_{i,\mu_i}|R_y\left(\frac{\langle h_i^{\mu_i}|H|h_i^{\mu_i}\rangle t}{\hbar}\right)|h_i^{\mu_i}\rangle +\\
&|a_1\rangle\bigotimes_\alpha|0_\alpha\rangle\langle 0_\alpha|R_y\left(\frac{\langle x_\alpha|H|x_\alpha\rangle t}{\hbar}\right)|x_\alpha\rangle\bigotimes_{i,\mu_i}|1_{i,\mu_i}\rangle\langle 1_{i,\mu_i}|R_y\left(\frac{\langle h_i^{\mu_i}|H|h_i^{\mu_i}\rangle t}{\hbar}\right)|h_i^{\mu_i}\rangle +\\
&|a_1\rangle\bigotimes_\alpha|1_\alpha\rangle\langle 1_\alpha|R_y\left(\frac{\langle x_\alpha|H|x_\alpha\rangle t}{\hbar}\right)|x_\alpha\rangle\bigotimes_{i,\mu_i}|0_{i,\mu_i}\rangle\langle 0_{i,\mu_i}|R_y\left(\frac{\langle h_i^{\mu_i}|H|h_i^{\mu_i}\rangle t}{\hbar}\right)|h_i^{\mu_i}\rangle +\\
&R_y\left(\frac{\langle x_\alpha|H|h_1^{\mu_1}\rangle}{\hbar}\right)|a_1\rangle\bigotimes_\alpha|1_\alpha\rangle\langle 1_\alpha|R_y\left(\frac{\langle x_\alpha|H|x_\alpha\rangle t}{\hbar}\right)|x_\alpha\rangle\bigotimes_{i,\mu_i}|1_{i,\mu_i}\rangle\langle 1_{i,\mu_i}|R_y\left(\frac{\langle h_i^{\mu_i}|H|h_i^{\mu_i}\rangle t}{\hbar}\right)|h_i^{\mu_i}\rangle +
\end{aligned} \tag{31}$$

The rotation angles of these doubly controlled R_y gates are parametrized by the weights in eq 11 and are different for different configurations of the control qubits. It must be emphasized that even though for a system requiring $n = m = 2$, one needs $n*m$ ancillary qubits, the total gate depth is 2 (constant), the circuit width is $O(n + m + mn)$, and the total number of gates is $O(n + m + mn)$ and so is the number of variational parameters in the model. Thus, the asymptotic scaling of all important metrics for the cost of the circuit is $polyn(n)$. However, an alternative implementation is possible

https://doi.org/10.1021/acs.jctc.3c00187
J. Chem. Theory Comput. 2023, 19, 2446−2454

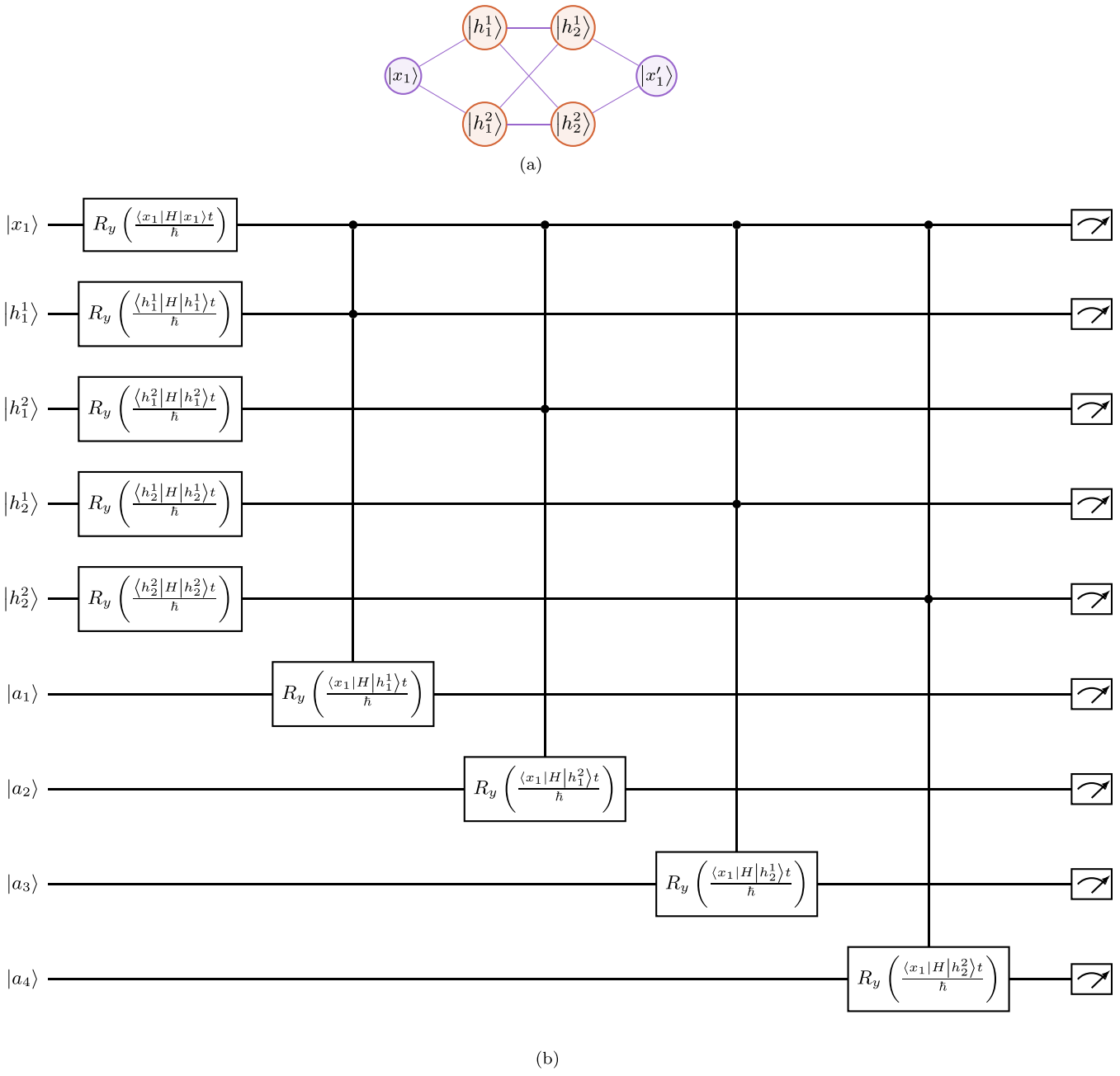

Figure 8. Illustration of the approach in Section 4 for two hidden layers and one input layer RBM system. The left visible layer is simply reproduced for convenience on the right side of panel (a). Panel (b) not only provides a circuit model for the neural in panel (a), but it also provides a circuit model for a Feynman path integral problem referred to in panel (a). The $|a_i\rangle$ represent the ancilla, $|x_i\rangle$ represent the visible layer (or end points of the Feynman path), and $|h_i\rangle$ are the hidden layers (or path elements that are used to construct the superposition in the Feynman path description).

too involving a single ancillary qubit which is reused $n*m$ times through midcircuit measurements. Since the measurement is conditioned on the collapse of this single ancilla in state $|1\rangle$ (only then phase-kickback ensures correct state on the data register), one can reset the ancilla to state $|0\rangle$ thereafter and reuse it for mediating the interaction between a different hidden and visible unit. However, in this scheme, the depth is $O(2mn)$ while the number of qubits required is $O(n + m + 1)$. A very different and yet another implementation of simulating a Restricted Boltzmann Machine is to directly prepare the Gibbs state of the Ising Model on a quantum device through a double optimization protocol as has been devised recently.[56] This scheme requires $O(n + m + 1)$ qubits, gate depth is D (variable usually $poly(n)$), and the number of quantum gates is $O(D*(n + m + 1))$. Thus, in short we can say that there are many different versions of quantum circuit now which can prepare a sampler from the RBM distribution. Even though the internal resource requirements of each may vary, but all of them have $O(poly(n))$ cost in number of qubits, number of gates, and depth.

9. CONCLUSION

Machine learning has had great impact recently in a number of areas of science. Recently, quantum versions of machine learning protocols have also been constructed. As machine learning grows in impact, there has been a wide discussion in the literature that deals with the interpretation of hidden layers as

https://doi.org/10.1021/acs.jctc.3c00187
J. Chem. Theory Comput. 2023, 19, 2446−2454

they appear in these formalisms. In this paper, we provide a general description for many problems in machine learning, and more precisely Boltzmann machines, by finding an analogy between these and the Feynman path integral description of quantum and statistical mechanics. We find that the basic mathematical structure of RBMs reminds us of a superposition of (or sum over) paths structure, which is a critical hallmark of Feynman's description of quantum and statistical mechanics. This then allows us to reinterpret the hidden layers in machine learning as being akin to the intermediate, or virtual, states visited by quantum systems as part of the path integration for quantum propagation in real and imaginary time. As a direct consequence of this argument, we are able to introduce a general quantum circuit that encompasses both RBMs and Feynman path integrals.

We then find that while 2-local Hamitonians within the Feynman path integral formalism are reminiscent of RBMs, *k*-local Hamiltonians naturally yield a structure that looks like a Boltzmann machine without restrictions. In fact, in such cases, the neural networks obtained look more like a simplical complex to allow connections that go beyond nearest neighbor of hidden layers. Given the isomorphism to graphs and simplicial complexes, we are also able to provide general expressions for entropy by applying the inclusion−exclusion principle directly to the simplicial complexes.

We have recently demonstrated[50] that how information between the two spin-registers of the network can flow in real-time during training and how such a finding can be leveraged to identify robust yet emergent training principles. We have further analytically related such information transport quantifiers to usual measures of correlation and have established rigorous bounds satisfied by the two quantities. A connection to Feynamn path integrals might shed light on such training dynamics and open a new path to analyze how footprints of quantum correlation within the physical system studied gets imprinted onto the learner network.

AUTHOR INFORMATION

Corresponding Authors

Srinivasan S. Iyengar − *Department of Chemistry and Indiana University Quantum Science and Engineering Center (IU-QSEC), Indiana University, Bloomington, Indiana 47405, United States;* orcid.org/0000-0001-6526-2907; Email: iyengar@indiana.edu

Sabre Kais − *Department of Chemistry, Department of Physics and Purdue Quantum Science and Engineering Institute, Purdue University, West Lafayette, Indiana 47907, United States;* orcid.org/0000-0003-0574-5346; Email: kais@purdue.edu

Complete contact information is available at: https://pubs.acs.org/10.1021/acs.jctc.3c00187

Notes

The authors declare no competing financial interest.

ACKNOWLEDGMENTS

This research was supported by the National Science Foundation Grants CHE-2102610 and OMA-1936353 to S.S.I. S.K. would like to thank Dr. Manas Sajjan for many useful discussions and acknowledges the National Science Foundation under Award No. 1955907 and the U.S. Department of Energy (Office of Basic Energy Sciences) under Award No. DESC0019215. S.S.I. acknowledges Mr. Xiao Zhu for his critical comments on the paper.

REFERENCES

(1) Christopher, M. *Bishop, Pattern Recognition and Machine Learning*; Springer: New York, 2006.

(2) Senior, A. W.; Evans, R.; Jumper, J.; Kirkpatrick, J.; Sifre, L.; Green, T.; Qin, C.; Zidek, A.; Nelson, A. W. R.; Bridgland, A.; Penedones, H.; Petersen, S.; Simonyan, K.; Crossan, S.; Kohli, P.; Jones, D. T.; Silver, D.; Kavukcuoglu, K.; Hassabis, D. Improved protein structure prediction using potentials from deep learning. *Nature* **2020**, *577*, 706−710.

(3) Jumper, J.; Evans, R.; Pritzel, A.; Green, T.; Figurnov, M.; Ronneberger, O.; Tunyasuvunakool, K.; Bates, R.; Zidek, A.; Potapenko, A.; Bridgland, A.; Meyer, C.; Kohl, S. A. A.; Ballard, A. J.; Cowie, A.; Romera-Paredes, B.; Nikolov, S.; Jain, R.; Adler, J.; Back, T.; Petersen, S.; Reiman, D.; Clancy, E.; Zielinski, M.; Steinegger, M.; Pacholska, M.; Berghammer, T.; Bodenstein, S.; Silver, D.; Vinyals, O.; Senior, A. W.; Kavukcuoglu, K.; Kohli, P.; Hassabis, D. Highly accurate protein structure prediction with alphafold. *Nature* **2021**, *596*, 583−589.

(4) Sajjan, M.; Li, J.; Selvarajan, R.; Sureshbabu, S. H.; Kale, S. S.; Gupta, R.; Singh, V.; Kais, S. Quantum machine learning for chemistry and physics. *Chem. Soc. Rev.* **2022**, *51*, 6475−6573.

(5) Wiebe, N.; Kapoor, A.; Svore, K. M. Quantum deep learning. *Quantum Information and Computation* **2016**, *16*, 541.

(6) Melko, R. G.; Carleo, G.; Carrasquilla, J.; Cirac, J. I. Restricted Boltzmann machines in quantum physics. *Nat. Phys.* **2019**, *15*, 887−892.

(7) Le Roux, N.; Bengio, Y. Representational Power of Restricted Boltzmann Machines and Deep Belief Networks. *Neural Computation* **2008**, *20*, 1631−1649.

(8) Nomura, Y.; Darmawan, A. S.; Yamaji, Y.; Imada, M. Restricted boltzmann machine learning for solving strongly correlated quantum systems. *Phys. Rev. B* **2017**, *96*, 205152.

(9) Carleo, G.; Nomura, Y.; Imada, M. Constructing exact representations of quantum many-body systems with deep neural networks. *Nat. Commun.* **2018**, *9*, 5322.

(10) Lee, C. K.; Patil, P.; Zhang, S.; Hsieh, C. Y. Neural-network variational quantum algorithm for simulating many-body dynamics. *Phys. Rev. Research* **2021**, *3*, 023095.

(11) Nandi, A.; Qu, C.; Houston, P. L.; Conte, R.; Bowman, J. M. δ machine learning for potential energy surfaces: A pip approach to bring a dft-based pes to ccsd(t) level of theory. *J. Chem. Phys.* **2021**, *154*, 051102.

(12) Nguyen, T. T.; Szekely, E.; Imbalzano, G.; Behler, J.; Csanyi, G.; Ceriotti, M.; Gotz, A. W.; Paesani, F. Comparison of permutationally invariant polynomials, neural networks, and gaussian approximation potentials in representing water interactions through many-body expansions. *J. Chem. Phys.* **2018**, *148*, 241725.

(13) Sajjan, M.; Sureshbabu, S. H.; Kais, S. Quantum machine-learning for eigenstate filtration in two-dimensional materials. *J. Am. Chem. Soc.* **2021**, *143*, 18426.

(14) Xia, R.; Kais, S. Quantum machine learning for electronic structure calculations. *Nat. Commun.* **2018**, *9*, 1−6.

(15) Kumar, A.; Iyengar, S. S. Fragment-based electronic structure for potential energy surfaces using a superposition of fragmentation topologies. *J. Chem. Theory Comput.* **2019**, *15*, 5769.

(16) Kumar, A.; DeGregorio, N.; Iyengar, S. S. Graph-theory-based molecular fragmentation for efficient and accurate potential surface calculations in multiple dimensions. *J. Chem. Theory Comput.* **2021**, *17*, 6671−6690.

(17) Zhu, X.; Iyengar, S. S. Graph theoretic molecular fragmentation for multidimensional potential energy surfaces yield an adaptive and general transfer machine learning protocol. *J. Chem. Theory Comput.* **2022**, *18*, 5125−5144.

(18) Kumar, A.; DeGregorio, N.; Ricard, T.; Iyengar, S. S. Molecular fragmentation with tensor networks for accurate quantum nuclear dynamics. *J. Chem. Theory Comput.* **2022**, *18*, 7243.

(19) Sahrmann, P. G.; Loose, T. D.; Durumeric, A. E. P.; Voth, G. A. Utilizing machine learning to greatly expand the range and accuracy of bottom-up coarse-grained models through virtual particles. *J. Chem. Theory Comput.* **2023**, na.
(20) Ciliberto, C.; Herbster, M.; Ialongo, A. D.; Pontil, M.; Rocchetto, A.; Severini, S.; Wossnig, L. Quantum machine learning: a classical perspective. *Proceedings of the Royal Society A: Mathematical, Physical and Engineering Sciences* **2018**, *474*, 20170551.
(21) Sohl-Dickstein, J.; Weiss, E. A.; Maheswaranathan, N.; Ganguli, S. Deep unsupervised learning using nonequilibrium thermodynamics. *arXiv Preprint*, arXiv:1503.03585, 2015.
(22) Deng, D.-L.; Li, X.; Das Sarma, S. Quantum entanglement in neural network states. *Phys. Rev. X* **2017**, *7*, 021021.
(23) Long, P. M.; Servedio, R. A.Restricted Boltzmann Machines are hard to approximately evaluate or simulate. In *ICML 2010 - Proceedings, 27th International Conference on Machine Learning*, 2010; pp 703−710.
(24) Zhang, J. H.; Iyengar, S. S. Graph-|Q⟩⟨C|: A graph-based quantum-classical algorithm for efficient electronic structure on hybrid quantum/classical hardware systems: Improved quantum circuit depth performance. *J. Chem. Theory Comput.* **2022**, *18*, 2885.
(25) Sager-Smith, L. M.; Mazziotti, D. A. Reducing the quantum many-electron problem to two electrons with machine learning. *J. Am. Chem. Soc.* **2022**, *144*, 18959−18966.
(26) Che, Y.; Gneiting, C.; Nori, F. Estimating the Euclidean quantum propagator with deep generative modelling of Feynman paths. *arXiv Preprint*, arXiv:2202.02750, 2022.
(27) Feynman, R. P.; Hibbs, A. R. *Quantum Mechanics and Path Integrals*; McGraw-Hill Book Company: New York, 1965.
(28) Feynman, R. P. *Statistical Mechanics*; Addison-Wesley: MA, 1972; Chap. 3.
(29) Klauder, J. R. The Feynman path integral: An historical slice. In *A Garden of Quanta*; World Scientific, 2003; pp 55−76.
(30) Kleinert, H. *Path Integrals in Quantum Mechanics, Statistics, Polymer Physics, and Financial Markets*, 5th ed. ; World Scientific, 2009.
(31) Makri, N. Feynman path integration in quantum dynamics. *Comput. Phys. Commun.* **1991**, *63*, 389.
(32) Kouri, D. J.; Zhu, W.; Ma, X.; Pettitt, B. M.; Hoffman, D. K. *J. Phys. Chem.* **1992**, *96*, 9622.
(33) Berne, B. J.; Thirumalai, D. On the simulation of quantum systems: Path integral methods. *Annu. Rev. Phys. Chem.* **1986**, *37*, 401.
(34) Chandler, D.; Wolynes, P. G. Exploiting the isomorphism between quantum theory and classical statistical mechanics of polyatomic fluids. *J. Chem. Phys.* **1981**, *74*, 4078.
(35) Tuckerman, M. E.; Marx, D.; Klein, M. L.; Parrinello, M. Efficient and general algorithms for path integral car-parrinello molecular dynamics. *J. Chem. Phys.* **1996**, *104*, 5579.
(36) Tuckerman, M. E.; Marx, D. Heavy-atom skeleton quantization and proton tunneling in "intermediate-barrier" hydrogen bonds. *Phys. Rev. Lett.* **2001**, *86*, 4946.
(37) Cao, J.; Voth, G. A. A new perspective on quantum time correlation functions. *J. Chem. Phys.* **1993**, *99*, 10070.
(38) Jang, S.; Voth, G. A. Path integral centroid variables and the formulation of their exact real time dynamics. *J. Chem. Phys.* **1999**, *111*, 2357.
(39) Jang, S.; Voth, G. A. A derivation of centroid molecular dynamics and other approximate time evolution methods for path integral centroid variables. *J. Chem. Phys.* **1999**, *111*, 2371.
(40) Habershon, S.; Manolopoulos, D. E.; Markland, T. E.; Miller, T. F. Ring polymer molecular dynamics: Quantum effects in chemical dynamics from classical trajectories in an extended phase space. *Annu. Rev. Phys. Chem.* **2013**, *64*, 387.
(41) Ju, Y.; Alam, S. S.; Minoff, J.; Anselmi, F.; Han, P.; Patel, A. Interpreting convolutional neural networks' low dimensional approximation to quantum spin systems. *arXiv Preprint*, arXiv:2210.00692, 2022.
(42) Monroe, C.; Campbell, W. C.; Duan, L.-M.; Gong, Z.-X.; Gorshkov, A. V.; Hess, P. W.; Islam, R.; Kim, K.; Linke, N. M.; Pagano, G.; Richerme, P.; Senko, C.; Yao, N. Y. Programmable quantum simulations of spin systems with trapped ions. *Rev. Mod. Phys.* **2021**, *93*, 025001.
(43) Labuhn, H.; Barredo, D.; Ravets, S.; de Leseleuc, S.; Macri, T.; Lahaye, T.; Browaeys, A. Tunable two-dimensional arrays of single rydberg atoms for realizing quantum ising models. *Nature* **2016**, *534*, 667−670.
(44) Yan, B.; Moses, S. A.; Gadway, B.; Covey, J. P.; Hazzard, K. R. A.; Rey, A. M.; Jin, D. S.; Ye, J. Observation of dipolar spin-exchange interactions with lattice-confined polar molecules. *Nature* **2013**, *501*, 521−525.
(45) Bloch, I.; Dalibard, J.; Nascimbene, S. Quantum simulations with ultracold quantum gases. *Nat. Phys.* **2012**, *8*, 267−276.
(46) Barends, R.; Shabani, A.; Lamata, L.; Kelly, J.; Mezzacapo, A.; Heras, U. L.; Babbush, R.; Fowler, A. G.; Campbell, B.; Chen, Y.; Chen, Z.; Chiaro, B.; Dunsworth, A.; Jeffrey, E.; Lucero, E.; Megrant, A.; Mutus, J. Y.; Neeley, M.; Neill, C.; O'Malley, P. J. J.; Quintana, C.; Roushan, P.; Sank, D.; Vainsencher, A.; Wenner, J.; White, T. C.; Solano, E.; Neven, H.; Martinis, J. M. Digitized adiabatic quantum computing with a superconducting circuit. *Nature* **2016**, *534*, 222−226.
(47) Newton, R. G. *Scattering Theory of Waves and Particles*; Springer-Verlag: New York, 1982.
(48) Björklund, A.; Husfeldt, T.; Koivisto, M. Set partitioning via inclusion exclusion. *SIAM J. Comput.* **2009**, *39*, 546.
(49) Yedidia, J. S.; Freeman, W. T.; Weiss, Y. Understanding belief propagation and its generalizations. In *Exploring Artificial Intelligence in the New Millennium*; Morgan Kaufmann Publishers, Inc.: San Francisco, CA, USA, 2003; pp 239−269.
(50) Sajjan, M.; Singh, V.; Selvarajan, R.; Kais, S. Imaginary components of out-of-time correlators and information scrambling for navigating the learning landscape of a quantum machine learning model. *Phys. Rev. Res.* **2023**, *5*, 013146.
(51) Dey, T. K.; Shah, N. R. On the number of simplicial complexes in rd. *Comput. Geom.* **1997**, *8*, 267.
(52) Armstrong, M. A. *Basic Topology*; Springer Science & Business Media, 2013.
(53) Ricard, T. C.; Iyengar, S. S. An efficient and accurate approach to estimate hybrid functional and large basis set contributions to condensed phase systems and molecule-surface interactions. *J. Chem. Theory Comput.* **2020**, *16*, 4790.
(54) Caldeira, A. O.; Leggett, A. J. Quantum tunnelling in a dissipative system. *Ann. Physics* **1983**, *149*, 374−456.
(55) Bermudez, A.; Tagliacozzo, L.; Sierra, G.; Richerme, P. Long-range heisenberg models in quasiperiodically driven crystals of trapped ions. *Phys. Rev. B* **2017**, *95*, 024431.
(56) Sajjan, M.; Alaeian, H.; Kais, S. Magnetic phases of spatially modulated spin-1 chains in rydberg excitons: Classical and quantum simulations. *J. Chem. Phys.* **2022**, *157*, 224111.

https://doi.org/10.1021/acs.jctc.3c00187
J. Chem. Theory Comput. 2023, 19, 2446−2454